

# Enhanced ponderomotive force in graphene due to interband resonance

**Wolff, C.; Tserkezis, C.; Mortensen, N. Asger**

*Published in:*
New Journal of Physics

*Link to article, DOI:*
10.1088/1367-2630/ab2f30

*Publication date:*
2019

*Document Version*
Publisher's PDF, also known as Version of record

PAPER • OPEN ACCESS

# Enhanced ponderomotive force in graphene due to interband resonance

New Journal of Physics
The open access journal at the forefront of physics

Deutsche Physikalische Gesellschaft DPG
IOP Institute of Physics

Published in partnership with: Deutsche Physikalische Gesellschaft and the Institute of Physics

OPEN ACCESS

RECEIVED
25 February 2019

REVISED
11 June 2019

ACCEPTED FOR PUBLICATION
3 July 2019

PUBLISHED
23 July 2019



PAPER

# Enhanced ponderomotive force in graphene due to interband resonance

C Wolff[1], C Tserkezis[1] and N Asger Mortensen[1,2,3]

[1] Center for Nano Optics, University of Southern Denmark, Campusvej 55, DK-5230 Odense M, Denmark
[2] Danish Institute for Advanced Study, University of Southern Denmark, Campusvej 55, DK-5230 Odense M, Denmark
[3] Center for Nanostructured Graphene, Technical University of Denmark, DK-2800 Kongens Lyngby, Denmark

**E-mail:** cwo@mci.sdu.dk

**Keywords:** graphene nonlinearities, ponderomotive force, nonlocal response

## Abstract

We analyze intrinsic nonlinearities in two-dimensional (2D) polaritonic materials interacting with an optical wave. Focusing on the case of graphene, we show that the second-order nonlinear optical conductivity due to carrier density fluctuations associated with the excitation of a plasmon polariton is closely related to the ponderomotive force due to the oscillating optical field. A recent study (Sun *et al* 2018 *Proc. Natl Acad. Sci. USA* **115** 3285–9) derived this force in the hydrodynamic regime of a generic Dirac fluid, and suggested that inclusion of interband transitions could have interesting implications. Here we reproduce the Drude-like result in a more general fashion on the basis of thermodynamics, which makes extension to other regimes straightforward. We find that for zero temperature a diverging nonlinearity is found at the interband threshold. By including finite-temperature effects this is regularized, but remains quite significant even at room temperature. Going further beyond, we include nonlocal corrections as a second potential source of regularization, and find that they do not lead to broadening (as one would usually expect e.g. due to Landau damping), but rather to a splitting of the ponderomotive interband resonance, providing a very characteristic signature of nonlocality. Our analysis should prove useful to the open quest for exploiting nonlinearities in graphene and other 2D polaritonic materials, through effects such as photon drag.

## 1. Introduction

The emergence of graphene [1, 2] and other two-dimensional (2D) materials [3, 4] at the forefront of research in all areas of condensed matter physics, owing to their intriguing mechanical [5], thermal [6], electronic [7] and optical properties [8], has led to a plethora of suggested applications, many of which are already starting to see the light of day. In photonics, in particular, where the possibility to excite and tailor highly confined polaritons can have important implications [9, 10], 2D materials became very quickly prominent templates for enabling and tailoring light–matter interactions [11–13]. In this context, the prospect of enhanced nonlinearities is always among the first effects to be explored in a novel architecture, and 2D materials could not fail to attract their share of attention [14–18].

In the long list of nonlinear optical effects, such as higher-harmonic generation, stimulated Raman and Rayleigh scattering, electrooptic effects and multiphoton absorption [19], ponderomotive effects are particularly relevant to plasmonics. Charged particles in inhomogeneous oscillating electromagnetic fields are known to be subject to a ponderomotive force proportional to the gradient of the electric field ($\vec{F} \propto \mathrm{grad}|\vec{E}|^2$) that accelerates them towards the field direction (see for example [20, 21] and reference therein). This has been exploited, for instance, for electron acceleration with laser pulses [22], and controlling excitons [23] or plasmons [24], as well as inducing nonlinear effects in them [25, 26]. With the advent of graphene as an exemplary plasmonic medium, it was only natural to explore its capability to enhance nonlinearities [27–29] such as second harmonic generation (SHG), which is usually symmetry-prohibited due to the high symmetry of the graphene lattice and therefore can only occur either at interfaces or if the optical excitation breaks symmetry either by oblique incidence or via intensity inhomogeneities.

In the former setting, a resonant enhancement at the interband threshold has been theoretically found recently [30] while the latter has been connected to the ponderomotive force [15].

Recently, the second-order nonlinear ac conductivity of a generic Dirac fluid was connected to the ponderomotive force through the hydrodynamic equations of motion [31]. As a directly available test bed, the authors of [31] applied their analysis to graphene, focusing on SHG and photon drag. Since their analysis was based on a hydrodynamic description, the authors restricted themselves to electromagnetic response at rather low frequencies (to be precise, $\omega \ll \Gamma_{ee}$, where $\Gamma_{ee}$ is the electron–electron scattering rate), yet at finite temperature $T$. Furthermore, they anticipated that at sufficiently high temperatures the interband contribution to the conductivity could become important even for the nonlinearity in the hydrodynamic regime. In this paper, we consider the effect of interband transitions directly excited by high-frequency optical waves at low to moderate temperatures on the ponderomotive force. We start by deriving the connection between the ac conductivity and the ponderomotive force with a different starting point, through a general and powerful thermodynamic approach which, to the best of our knowledge, has not been presented before. By introducing the second-order, room-temperature expression for the conductivity of graphene, we show that the resulting ponderomotive force exhibits a resonance at an energy twice the Fermi energy, becoming infinite at zero temperature. This resonant behavior survives for higher temperatures, and can lead to forces as large as one order of magnitude stronger than in the intraband case, over a relatively wide energy range.

## 2. Preliminaries

We consider a graphene monolayer sandwiched between two dielectrics with relative permittivities $\varepsilon_1$ and $\varepsilon_2$. Within a local response approximation, the electromagnetic properties of graphene are characterized by a complex sheet conductance $\sigma(\omega)$. It has two contributions ($\sigma = \sigma_1 + \sigma_2$): firstly a Drude model

$$\frac{\sigma_1(\omega)}{\sigma_K} = \frac{\mathrm{i}2\mathscr{E}_F}{\hbar\,[\omega + \mathrm{i}\gamma(\omega)]}, \tag{1}$$

due to intraband scattering of free carriers. It is characterized by an Ohmic damping $\gamma(\omega)$ due to the scattering of carriers predominantly off lattice impurities at low temperatures and phonons at higher temperatures. The frequency dependence is generally required in order to ensure that the local electron density is conserved [32]. In the context of our work, this is of no consequence and for simplicity, we suppress this in the remainder. The second contribution describes the effect of interband transitions if the photon energy $\hbar\omega$ exceeds twice the Fermi energy $\mathscr{E}_F$ (relative to the undoped state). At zero temperature. it takes the form:

$$\frac{\sigma_2^{(T=0)}(\omega)}{\sigma_K} = \frac{\pi}{2}\left[\Theta(\hbar\omega - 2\mathscr{E}_F) + \frac{\mathrm{i}}{\pi}\ln\left|\frac{\hbar\omega - 2\mathscr{E}_F}{\hbar\omega + 2\mathscr{E}_F}\right|\right]. \tag{2}$$

Here, $\hbar$ is Planck's constant, $\Theta(x)$ is the Heaviside function, and $\sigma_K = e^2/h \simeq 3.87 \times 10^{-5}$ S is the inverse of the von-Klitzing constant, with $e$ being the electron charge [11].

The full optical conductivity of graphene at finite temperature has been calculated in [33, 34]

$$\frac{\sigma^{(T>0)}(\omega)}{\sigma_K} = \frac{\mathrm{i}2\mathscr{E}_F}{\hbar\,(\omega + \mathrm{i}\gamma)} + \frac{\pi}{4}\left(\tanh\frac{\hbar\omega + 2\mathscr{E}_F}{4k_BT} + \tanh\frac{\hbar\omega - 2\mathscr{E}_F}{4k_BT} + \frac{\mathrm{i}}{\pi}\ln\frac{(\hbar\omega - 2\mathscr{E}_F)^2 + (2k_BT)^2}{(\hbar\omega + 2\mathscr{E}_F)^2}\right), \tag{3}$$

where $k_B$ is the Boltzmann constant and $T$ the temperature. This expression can be further corrected through appropriate multiplicative factors proportional to the square of the energy over the hopping parameter of the tight-binding description of graphene [33]. However, this correction is usually of minor importance [27, 34], and our calculations showed that it can be safely disregarded here as well.

Graphene is best known and has received most of its attention because of its linear energy-momentum relation at the undoped Fermi energy [11]. This implies that the common expression $m_{\mathrm{eff}} = \hbar^2[\partial^2\mathscr{E}/\partial k^2]^{-1}$ for the electron effective mass is ill-defined for its quasiparticles, which in fact have vanishing 'rest mass'. Instead, the appropriate expression for the effective mass is the dynamic mass of a relativistic massless particle, where the energy-independent Fermi velocity $v_F$ takes the role of the speed of light [1]:

$$\mathscr{E} = m_{\mathrm{eff}}\,v_F^2. \tag{4}$$

In further analogy to relativistic massless particles, the Fermi wave number $q_F$ is related to the Fermi energy via the linear relationship

$$\mathscr{E}_F = \hbar v_F q_F. \tag{5}$$

Finally, the Fermi wave number is directly connected to the density $n$ of free carriers:

$$q_{\mathrm{F}} = \sqrt{\pi n}\,. \tag{6}$$

Here, we study how a plasmon polariton and an optical wave interact in a graphene sheet due to the intrinsic nonlinearity of graphene. To this end, we introduce a separation of scales. The optical wave is assumed to oscillate at an angular frequency $\omega$, whereas the polariton oscillates at an angular frequency $\Omega \ll \omega$. As a result, the optical parameters can be assumed to be modified by the polariton, but remain quasi-stationary as far as the optical wave is concerned. This separation of frequency scales is intrinsic to the notion of the ponderomotive force.

Within this work, we employ a thermodynamic argument based on the free enthalpy $\mathscr{G}$ to obtain an expression for the ponderomotive force. It requires the electron distribution to remain near the thermal equilibrium. This assumption is compatible with the assumption of a very slow, long-wavelength polariton, which quasi-adibatically modifies the electronic system. As for the optical excitation, we note that it certainly changes the occupation of the electron levels that are responsible for the permittivity at this optical frequency. In the case of interband transitions for example, the non-thermal distribution features excess carriers in the destination states [35]. This means that an electron system far away from thermal equilibrium is bound to exhibit a quasi-instantaneous Kerr nonlinearity (e.g. saturation in the example of interband transitions) assuming the carrier density is kept constant. But assuming linear response in equation (3), we have implicitly assumed a quasi-thermal electron distribution, which justifies our approach.

## 3. Intraband contribution to nonlinear response

First, we derive the ponderomotive force ignoring interband transitions. The basic idea is that a plasmon polariton is in essence a fluctuation in the carrier density, and therefore accompanied by a spatial modulation of the local Fermi level $\mathscr{E}_{\mathrm{F}}$. The notion of a local Fermi level is acceptable as long as the polaritonic wavelength is large enough to ensure the electron system to reach a local equilibrium, i.e. whenever local response theory applies. This is the case if it is large compared to the electronic mean free path length. As a rough estimate, the ratio of damping constant and Fermi velocity point at the order of 100 nm or shorter. It also implies the assumption that the polariton does not cause too much 'unrest' in the electron system, but rather moves carriers around in a quasi-adiabatic way while overall maintaining the general shape of the Fermi distribution. This can be expected whenever the polariton experiences low loss, as any qualitative distortion of the Fermi distribution really means dissipation. The Fermi level in turn controls the intraband conductance of graphene through equation (1) and is linked to the total carrier density through equation (6). This means that we can estimate the change to the optical response simply through the chain rule:

$$\frac{\partial \sigma_1}{\partial n} = \frac{\partial \sigma_1}{\partial \mathscr{E}_{\mathrm{F}}}\frac{\partial \mathscr{E}_{\mathrm{F}}}{\partial n} = \frac{\mathrm{i}e^2 v_{\mathrm{F}}}{2\hbar\,(\omega + \mathrm{i}\gamma)\,\sqrt{\pi n}} = \frac{\sigma_1}{2n}. \tag{7}$$

We now aim to gain a better understanding of the expression equation (7) for the polariton-induced change to the optical properties. To this end, we recall the definition of a permittivity from the total free enthalpy $\mathscr{G}$ of a solid [20]:

$$[\varepsilon_r]_{ij} = -\frac{1}{\varepsilon_0}\cdot\frac{\partial^2 \mathscr{G}}{(\partial E_i)(\partial E_j)}. \tag{8}$$

Using the relationship $\sigma = -\mathrm{i}\omega\varepsilon_0\varepsilon_r$ between the complex conductance and the permittivity of a material, we can adapt equation (8) to the case of an isotropic sheet conductance:

$$\sigma = \mathrm{i}\omega\frac{\partial^2 \mathscr{G}}{\partial |\vec{E}_{\parallel}|^2}, \tag{9}$$

where $\vec{E}_{\parallel}$ is the tangential field at the position of the sheet. The fact that $\vec{E}_{\parallel}$ is continuous across the sheet motivates why $\vec{E}$ was chosen as the independent variable[4] in equation (8).

Using equation (9), we can characterize the intrinsic second-order nonlinearity of graphene by a parameter $W$ via:

[4] Strictly speaking, our thermodynamic potential $\mathscr{G}$ is not the free enthalpy, which is defined with the electric induction $\vec{D}$ as the independent variable and connected to $\mathscr{G}$ via a Legendre transformation [20]. This detail is of no concern for our argument.

$$W = \frac{\partial}{\partial n}\left[\frac{\partial^2 \mathscr{G}}{\partial |\vec{E}_\parallel|^2}\right] = \frac{\sigma_1}{2\mathrm{i}n\omega}. \tag{10}$$

Under the assumption that this nonlinear process in itself is reversible, we can interchange the order of derivatives and also find

$$W = \frac{\partial^2}{\partial |\vec{E}_\parallel|^2}\left[\frac{\partial \mathscr{G}}{\partial n}\right]. \tag{11}$$

This time, the term in brackets is the definition of a local chemical potential, so equation (11) describes a correction to the chemical potential caused by a change in the intensity of a quickly oscillating electric field. This is of course just a Maxwell relation and intimately related to the Manley–Rowe relations known from nonlinear optics and electrical engineering [19]. Even though it sounds similar to our starting point (change of the Fermi level due to a propagating polariton), it describes in fact the inverse process. Again, it should be stressed that this conclusion requires the nonlinear interaction to be reversible, i. e.not to create any entropy, not to be dissipative. Therefore, we can expect this to hold exactly in the limit $\gamma = 0$ and gradually be broken as $\gamma$ assumes a finite value.

From equation (7), we can see that $W$ does not depend on the electric field, so we can derive from equation (11) an explicit expression for the change in chemical potential

$$\Delta\mu = \frac{\partial \mathscr{G}}{\partial n} = W|\vec{E}_\parallel|^2. \tag{12}$$

This exerts a force on each particle that is proportional to the in-plane gradient:

$$\vec{F}_1 = \mathrm{grad}_\parallel(\Delta\mu) = \frac{\sigma_1}{2\mathrm{i}n\omega}\,\mathrm{grad}_\parallel|\vec{E}_\parallel|^2, \tag{13}$$

where $\mathrm{grad}_\parallel$ represents the 2D gradient operator in the sheet plane. Finally, in the limit of vanishing loss ($\gamma \to 0$) and using equations (4)–(6)), we find:

$$\vec{F} = \frac{e^2}{2m_{\mathrm{eff}}\omega^2}\,\mathrm{grad}_\parallel|\vec{E}_\parallel|^2. \tag{14}$$

This is the expression for the ponderomotive force in a 2D plasma composed of particles with effective mass $m_{\mathrm{eff}}$. Therefore, we have established that the intrinsic nonlinear change of the optical conductance due to a plasmon polariton in a graphene sheet is the complementary process to the ponderomotive force through which variations in the intensity of an optical field can drive polaritons.

A similar expression was recently derived in [31], albeit with a different starting point and analysis, and restricted to the intraband scattering region. Nevertheless, the authors of [31] did stress the necessity to explore interband corrections, already proven to be capable of enhancing third-order nonlinearities [36] or contributing to difference frequency generation [37], and this is what we shall do in the next section.

## 4. Interband contribution

The connection we established in the previous section now allows us to find the generalized ponderomotive force in situations where the electron system can no longer be described as a Drude plasma. This is for example the case in the regime $2\hbar\omega > \mathscr{E}_{\mathrm{F}}$, where the electromagnetic response is significantly modified by interband transitions. Following our previous analysis, we can express the correction to the ponderomotive force in terms of the density derivative of the interband conductance, provided this nonlinear coefficient describes a reversible process. For optical frequencies $\omega \neq 2\mathscr{E}_{\mathrm{F}}/\hbar$, we find:

$$\vec{F}_2^{(T=0)} = \frac{1}{\mathrm{i}\omega}\cdot\frac{\partial\sigma_2^{(T=0)}}{\partial n}\,\mathrm{grad}_\parallel|\vec{E}_\parallel|^2 \tag{15}$$

$$= \frac{-e^2}{2m_{\mathrm{eff}}[\omega^2 - (2\mathscr{E}_{\mathrm{F}}/\hbar)^2]}\,\mathrm{grad}_\parallel|\vec{E}_\parallel|^2. \tag{16}$$

This expression is purely real-valued, i.e. the variation in the Fermi level does not lead to a change in the absorptivity of the material unless the optical frequency is chosen such that $\hbar\omega - 2\mathscr{E}_{\mathrm{F}}$ changes sign. Only in this case, the nonlinearity features a substantial imaginary part, i.e. becomes dissipative. Otherwise, equation (16) constitutes a real ponderomotive force. Due to the resonant nature of equation (16), this force diverges as the optical frequency approaches the interband threshold from either side, especially from the low-loss side. In theory, the ponderomotive forces per unit of optical intensity can be made arbitrarily large by moving towards the point $\omega = 2\mathscr{E}_{\mathrm{F}}/\hbar$. This divergence is of course just an artifact of assuming the step-like Fermi distribution at zero temperature and will be regularized for any $T \neq 0$.

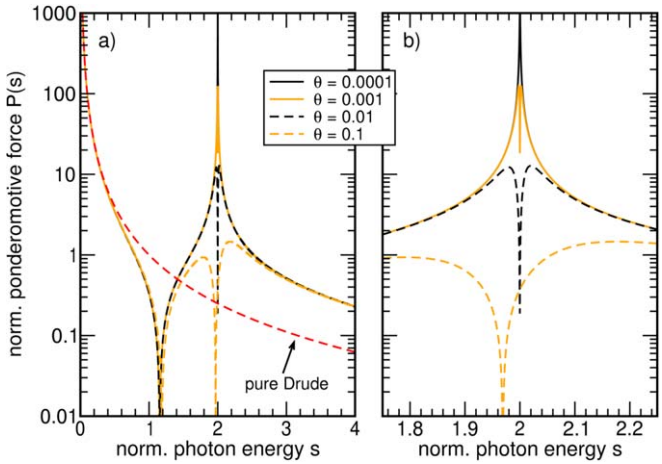


**Figure 1.** Dependence (overview in panel (a), close-up of the interband resonance in panel (b) of the frequency-part $P(s)$ of the finite-temperature ponderomotive force as defined in equation (19) on the normalized photon energy $s = \hbar\omega/\mathscr{E}_\mathrm{F}$ for the annotated values of the normalized temperature $\theta = k_\mathrm{B}T/\mathscr{E}_\mathrm{F}$. For $\mathscr{E}_\mathrm{F} = 893$ meV, the temperatures correspond to 1, 10, 100, and 1000 K, respectively. The red dashed line indicates the pure Drude-like ponderomotive force without interband contributions for comparison. It should be pointed out that this logarithmic plot does not reflect the sign of the ponderomotive force, which undergoes a change from negative to positive across the interband resonance.

Indeed, starting from equation (3), we find that the real pole turns into a Lorentzian imaginary part:

$$\frac{1}{\sigma_\mathrm{K}}\frac{\partial\sigma_2^{(T>0)}}{\partial\mathscr{E}_\mathrm{F}} = \frac{\pi}{8k_\mathrm{B}T}\left[\mathrm{sech}^2\frac{\hbar\omega+2\mathscr{E}_\mathrm{F}}{4k_\mathrm{B}T} - \mathrm{sech}^2\frac{\hbar\omega-2\mathscr{E}_\mathrm{F}}{4k_\mathrm{B}T}\right] - \frac{\mathrm{i}}{\hbar\omega+2\mathscr{E}_\mathrm{F}} - \frac{\mathrm{i}(\hbar\omega-2\mathscr{E}_\mathrm{F})}{(\hbar\omega-2\mathscr{E}_\mathrm{F})^2+(2k_\mathrm{B}T)^2}. \quad (17)$$

Due to the more broadband loss of interband transitions at finite temperature, this derivative is non-real everywhere, so strictly speaking, it does not provide a real ponderomotive force. However, at least in parameter ranges where the real part of equation (17) is small, we can regard inserting its imaginary part in equation (15) to be a good approximation:

$$\vec{F}_2^{(T>0)} \approx \frac{-\hbar e^2}{4\omega m_\mathrm{eff}}\left[\frac{\hbar\omega-2\mathscr{E}_\mathrm{F}}{(\hbar\omega-2\mathscr{E}_\mathrm{F})^2+(2k_\mathrm{B}T)^2} + \frac{1}{\hbar\omega+2\mathscr{E}_\mathrm{F}}\right]\mathrm{grad}_\parallel|\vec{E}_\parallel|^2. \quad (18)$$

It is natural to relate both the photon energy $\hbar\omega$ and temperature $T$ to the Fermi energy in order to obtain a more universal expression. Introducing the normalized quantities $s = \hbar\omega/\mathscr{E}_\mathrm{F}$ and $\theta = k_\mathrm{B}T/\mathscr{E}_\mathrm{F}$, we find for the total ponderomotive force:

$$\vec{F}_\mathrm{tot}^{(T>0)} = \overbrace{\frac{\hbar^2e^2}{4m_\mathrm{eff}\mathscr{E}_\mathrm{F}^2}\mathrm{grad}_\parallel|\vec{E}_\parallel|^2\cdot\frac{1}{s^2}}^{=\vec{F}_\mathrm{I}(s)/2}\cdot\underbrace{\left[2-\frac{s(s-2)}{(s-2)^2+4\theta^2}-\frac{s}{s+2}\right]}_{=P(s)}, \quad (19)$$

where the factor outside the bracket turns out to be the Drude-like intraband ponderomotive force $\vec{F}_\mathrm{I}$ as indicated. The dimensionless function $P(s)$ summarizes the frequency-dependence and describes the ponderomotive force normalized to all appearing fundamental constants and the electric field gradient. In figure 1, we show $P(s)$ for a number of normalized temperatures $\theta$.

## 5. Nonlocal corrections

For completeness, we finally present the main effect of nonlocality to the ponderomotive force at finite temperature. Since the ponderomotive force describes a nonlinearity, terms like 'nonlocality' or 'inhomogeneity' require clarification to avoid confusion. We consider the dependence of the ponderomotive force on the *optical* wave vector $\vec{k}_\parallel$ projected to the sheet plane. In analogy to the scale separation in time mentioned in the preliminaries, we assume that the length scale of the charge distribution (i.e. the wavelength of the polariton) is large compared to $\vec{k}_\parallel$. It should be noted that this is not necessarily as good an assumption as the time-scale separation, because of the high confinement of the plasmon polaritons.

To the best of our knowledge, there is no model for the nonlocal effect in the intraband (Drude-like) conductance that is both applicable beyond the interband threshold ($s > 2$) and conducive for the style of analytical calculations we present in this paper. Therefore, we restrict ourselves to the effect of nonlocality on the interband case, which is anyway potentially of greater interest, because of its resonant nature.

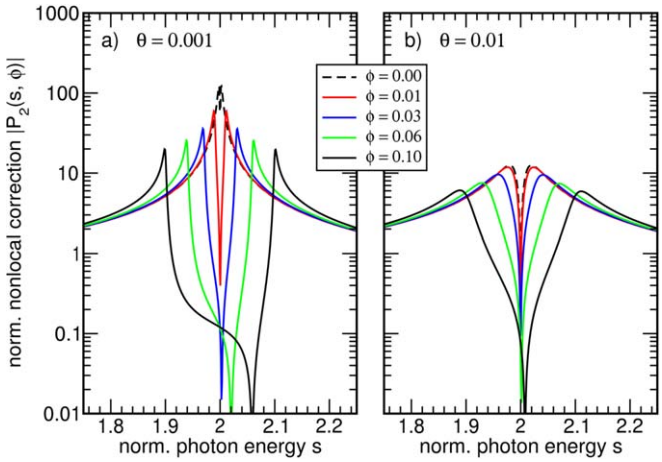


**Figure 2.** Effect of nonlocality on the interband contribution to the ponderomotive force (equation (5)) at two normalized temperatures (panel (a): $\theta = 0.001$; panel (b): $\theta = 0.01$) and for several values of $k_\parallel$ corresponding to different angles of incidence $\phi = k_\parallel/k_F$ of the driving light field.

The origin of the nonlocal interband effect is the conservation of momentum, where we assume a large graphene sheet and homogeneous optical illumination (spatially slowly varying envelope): a carrier from the lower branch of the dispersion relation with an initial wave vector on the circle $|\vec{q}_{in}| = q_0$ is not lifted to the same wave vector on the upper branch, but to a final wave vector on the circle that is shifted by the optical wave vector $\vec{k}_\parallel$: $|\vec{q}_{fin} - \vec{k}_\parallel| = q_0$. As a result, the effective interband transition energy is no longer independent of the exact wave number on the initial wave number circle, but offset by up to $\pm v_F \vec{k}_\parallel$. Since all source states with the same energy form a circle in $\vec{k}$-space, we find for the nonlocally corrected conductance:

$$\sigma_2(\omega, k_\parallel) = \frac{1}{\pi}\int_{-\pi}^{0} \mathrm{d}\alpha\ \sigma_2(\omega + v_F k_\parallel \cos\alpha), \tag{20}$$

where the conductivity under the integral is the local conductivity and only the modulus $k_\parallel$ of the optical wave vector matters because of the cylindrical symmetry of the Dirac cone. This smearing effect carries through the entire derivation and does not interact with the partial derivatives leading to the ponderomotive force. Hence, we find for the interband ponderomotive force including nonlocal corrections:

$$\vec{F}_2(\omega, k_\parallel) = \frac{1}{\pi}\int_{-1}^{1} \mathrm{d}z\ \frac{\vec{F}_2(\omega + v_F k_\parallel z)}{\sqrt{1 - z^2}}, \tag{21}$$

with $z = \cos\alpha$. We only study the seemingly more complex case of finite temperature, because at $T = 0$, there is a pole in the integration interval, which means that the zero temperature case must be obtained as the limit $T \to 0$ of the finite temperature expression. As before, we choose to separate the normalized frequency dependence from constants that clutter the notation by generalizing the inter-band contribution $P_2(s)$ to the normalized response function $P(s)$:

$$P_2(s, \phi) = \frac{1}{\pi}\int_{-1}^{1} \mathrm{d}z\ \frac{P_2(s + \phi z)}{\sqrt{1 - z^2}}, \tag{22}$$

where $\phi = k_\parallel/k_F$ is the normalized in-plane optical wave number and therefore simultaneously parameterizes the optical phase velocity and angle of incidence. As far as we can tell, equation (22) has no closed solution in terms of fundamental functions, but under the assumptions $s \approx 2$ and $\phi \ll 1$ ($c \gg v_F$), we can approximate it (see appendix for details):

$$P_2(s, \phi) = 2I(s, \phi, -2), +I(s, \phi, 2 + 2\mathrm{i}\theta) + I(s, \phi, 2 - 2\mathrm{i}\theta) \tag{23}$$

with

$$I(s, \phi, A) \approx \frac{(2s - A)\,\mathrm{sgn}\,(\Re\{s - A\})}{2s^2\sqrt{(s - A)^2 - \phi^2}} - \frac{1}{2s^2}, \tag{24}$$

where sgn $(\Re\{z\}) = x/|x|$ for $z = x + iy$. We find that this approximate expression matches a direct numerical integration of equation (22) very well within in the range $1.5 \leqslant s \leqslant 2.5$ and $\phi \leqslant 0.1$, which corresponds to an optical wavenumber ten times higher than in vacuum.

In figure 2, we show equation (24) for two normalized temperatures and a number of normalized in-plane wave numbers. We find that the effect of the interband nonlocality on the ponderomotive force differs significantly from most nonlocal corrections found in plasmonics. Usually, nonlocality leads to spectral shifts as well as additional damping and smearing of spectral features e.g. due to Landau damping [38]. Instead, we find a splitting of the ponderomotive resonance in the regime $\phi > \theta$ corresponding to $k_{\parallel} > k_{\mathrm{B}} T/\hbar v_{\mathrm{F}}$. Below this threshold, the splitting exists in principle, but is hidden by thermal broadening.

## 6. Conclusion

In summary, we derived an expression for the ponderomotive force arising from the optical excitation of a polariton in a 2D material, focusing our analysis on the case of graphene. Starting from a thermodynamic approach that relates the material permittivity to the total free enthalpy, we obtained a general relation between the ponderomotive force and the 2D sheet conductivity. By introducing into this the appropriate expression for the interband graphene conductivity, we showed that the resulting ponderomotive force exhibits a pole, which leads to its divergence at zero temperature. At higher temperatures, this divergence is gradually smoothed, but there is always an energy region around half the Fermi energy where the interband contribution is larger than the corresponding Drude part. This can play an important role when exploring second-order intrinsic nonlinearities in polaritonic materials, as for example in the recent study of stimulated plasmon polariton scattering [39]. Finally, we explored the impact of nonlocal corrections to the interband part assuming a spatially slowly varying optical envelope, and found a very characteristic type of resonance splitting. Strikingly, this is very distinct from the simple broadening and minuscule resonance shifts, which are the most common type of nonlocal correction in linear plasmonics [40–42], and therefore a very clear signature for nonlocal response in plasmonics.

## Acknowledgments

CW acknowledges funding from a MULTIPLY fellowship under the Marie Skłodowska-Curie COFUND Action (grant agreement No. 713694). CW also acknowledges controversial yet fruitful discussions with Dr Wolff. The Center for Nano Optics is financially supported by the University of Southern Denmark (SDU 2020 funding). NAM is a VILLUM Investigator supported by VILLUM Fonden (grant No. 16498). The Center for Nanostructured Graphene is sponsored by the Danish National Research Foundation (Project No. DNRF103).

## Appendix. Analytic approximation to the nonlocal correction

Here, we find an approximate solution to the integral

$$P_2(s,\,\phi) = \frac{1}{\pi}\int_{-1}^{1} \mathrm{d}z\, \frac{1}{\sqrt{1-z^2}}\frac{1}{s+\phi z}\left[\frac{s+\phi z-2}{(s+\phi z-2)^2+4\theta^2}+\frac{1}{s+\phi z+2}\right] \tag{A.1}$$

$$= \frac{1}{2\pi}\int_{-1}^{1} \mathrm{d}z\, \frac{1}{\sqrt{1-z^2}}\cdot\frac{1}{s+\phi z}\left[\frac{1}{s+\phi z-2+2\mathrm{i}\theta}+\frac{1}{s+\phi z-2-2\mathrm{i}\theta}+\frac{2}{s+\phi z+2}\right]. \tag{A.2}$$

This partial fraction decomposition reduces the problem to three integrals of the same form

$$I(s,\,\phi,\,A) = \frac{1}{2\pi}\int_{-1}^{1} \mathrm{d}z\, \frac{1}{\sqrt{1-z^2}}\cdot\frac{1}{s+\phi z}\cdot\frac{1}{s+\phi z-A}. \tag{A.3}$$

Next, we restrict ourselves to the neighborhood of the inter-band resonance, i.e. $s \approx 2$ and we assume $\phi \ll 1$. This means we may approximate $(s+\phi z)^{-1} \approx s^{-2}(s-\phi z)$:

$$I(s,\,\phi,\,A) \approx \frac{1}{2\pi s^2}\int_{-1}^{1} \mathrm{d}z\, \frac{1}{\sqrt{1-z^2}}\cdot\frac{s-\phi z}{\phi z+s-A} \tag{A.4}$$

$$= \frac{1}{2\pi s^2}\int_{-1}^{1} \mathrm{d}z\ \frac{1}{\sqrt{1-z^2}}\left[\frac{2s-A}{\phi z + s - A} - 1\right] \tag{A.5}$$

$$= \frac{-1}{2s^2} + \frac{2s-A}{2\pi\phi s^2}\int_{-1}^{1} \mathrm{d}z\ \frac{1}{(z+a)\sqrt{1-z^2}}, \tag{A.6}$$

with $a = (s - A)/\phi$. This is a standard integral and evaluates to $\pi/\sqrt{a^2-1}$. The expression is ambiguous as to which branch of the root function is to be used. This is solved by identifying the integration result at $\phi = 0$ with the local expression $P_2(s)$. In this way, we arrive at equation (5).

## ORCID iDs

C Wolff https://orcid.org/0000-0002-5759-6779
C Tserkezis https://orcid.org/0000-0002-2075-9036
N Asger Mortensen https://orcid.org/0000-0001-7936-6264

## References

[1] Castro Neto A H, Guinea F, Peres N M R, Novoselov K S and Geim A K 2009 The electronic properties of graphene *Rev. Mod. Phys.* **81** 109–62
[2] Ferrari A C *et al* 2015 Science and technology roadmap for graphene, related two-dimensional crystals, and hybrid systems *Nanoscale* **7** 4598–810
[3] Xu M, Liang T, Shi M and Chen H 2013 Graphene-like two-dimensional materials *Chem. Rev.* **113** 3766–98
[4] Butler S Z *et al* 2013 Progress, challenges, and opportunities in two-dimensional materials beyond graphene *ACS Nano* **7** 2898–926
[5] Frank I W, Tanenbaum D M, van der Zande A M and McEuen P L 2007 Mechanical properties of suspended graphene sheets *J. Vac Sci. Technol.* B **25** 2558–61
[6] Balandin A A 2011 Thermal properties of graphene and nanostructured carbon materials *Nat. Nanotechnol.* **10** 569–81
[7] Fiori G, Bonaccorso F, Iannaccone G, Palacios T, Neumaier D, Seabaugh A, Banerjee S K and Colombo L 2014 Electronics based on two-dimensional materials *Nat. Nanotechnol.* **9** 768–79
[8] Xia F, Wang H, Xiao D, Dubey M and Ramasubramaniam A 2014 Two-dimensional material nanophotonics *Nat. Photon.* **8** 899–907
[9] Mills D L and Burstein E 1974 Polaritons: the electromagnetic modes of media *Rep. Prog. Phys.* **37** 817–926
[10] Zayats A V and Smolyaninov I I 2003 Near-field photonics: surface plasmon polaritons and localized surface plasmons *J. Opt. A: Pure Appl. Opt.* **5** S16–50
[11] Gonçalves P A D and Peres N M R 2016 *An Introduction to Graphene Plasmonics* (Singapore: World Scientific)
[12] Xiao S, Zhu X, Li B-H and Mortensen N A 2016 Graphene-plasmon polaritons: From fundamental properties to potential applications *Frontiers Phys.* **11** 117801
[13] Low T *et al* 2017 Polaritons in layered two-dimensional materials *Nat. Mater.* **16** 182–94
[14] Hendry E, Hale P J, Moger J, Savchenko A K and Mikhailov S A 2010 Coherent nonlinear optical response of graphene *Phys. Rev. Lett.* **105** 097401
[15] Gullans M, Chang D E, Koppens F H L, García de Abajo F J and Lukin M D 2013 Single-photon nonlinear optics with graphene plasmons *Phys. Rev. Lett.* **111** 247401
[16] Rodríguez Echarri A, Cox J D, Yu R and García de Abajo F J 2018 Enhancement of nonlinear optical phenomena by localized resonances *ACS Photonics* **5** 1521–7
[17] Cheng J L, Sipe J E, Vermeulen N and Guo C 2018 Nonlinear optics of graphene and other 2d materials in layered structures *J. Phys.: Photonics* **1** 015002
[18] You J W, Bongu S R, Bao Q and Panoiu N C 2019 Nonlinear optical properties and applications of 2d materials: theoretical and experimental aspects *Nanophotonics* **8** 63–97
[19] Boyd R W 2003 *Nonlinear Optics* 3rd edn (New York: Academic)
[20] Landau L D, Lifshitz E M and Pitaevskii L P 1984 Electrodynamics of continuous media *Course of Theoretical Physics* 2nd edn (Oxford: Butterworth)
[21] Aliev Y M, Bychenkov V Y, Jovanovi M S and Frolov A A 1992 The kinetic theory of the nonlinear low-frequency response of a collisionless plasma to high-frequency electromagnetic radiation *J. Plasma Phys.* **48** 167–76
[22] Malka G and Miquel J L 1996 Experimental confirmation of ponderomotive-force electrons produced by an ultrarelativistic laser pulse on a solid target *Phys. Rev. Lett.* **77** 75–8
[23] Leinß S, Kampfrath T, von Volkmann K, Wolf M, Steiner J T, Kira M, Koch S W, Leitenstorfer A and Huber R 2008 Terahertz coherent control of optically dark paraexcitons in $cu_2O$ *Phys. Rev. Lett.* **101** 246401
[24] Irvine S D, Dombi P, Farkas G and Elezzabi A Y 2006 Influence of the carrier-envelope phase of few-cycle pulses on ponderomotive surface-plasmon electron acceleration *Phys. Rev. Lett.* **97** 146801
[25] Johnsen K and Jauho A-P 1999 Quasienergy spectroscopy of excitons *Phys. Rev. Lett.* **83** 1207–10
[26] Ginzburg P, Hayat A, Berkovitch N and Orenstein M 2010 Nonlocal ponderomotive nonlinearity in plasmonics *Opt. Lett.* **35** 1551–3
[27] Mikhailov S A 2011 Theory of the giant plasmon-enhanced second-harmonic generation in graphene and semiconductor two-dimensional electron systems *Phys. Rev.* B **84** 045432
[28] Hong S-Y, Dadap J I, Petrone N, Yeh P-C, Hone J and Osgood R M Jr 2013 Optical third-harmonic generation in graphene *Phys. Rev.* X **3** 021014
[29] Cheng J L, Vermeulen N and Sipe J E 2014 Dc current induced second order optical nonlinearity in graphene *Opt. Express* **22** 15868–76
[30] Cheng J L, Vermeulen N and Sipe J E 2017 Second order optical nonlinearity of graphene due to electric quadrupole and magnetic dipole effects *Sci. Rep.* **7** 43843
[31] Sun Z, Basov D N and Fogler M M 2018 Universal linear and nonlinear electrodynamics of a dirac fluid *Proc. Natl Acad. Sci. USA* **115** 3285–9
[32] Mermin N D 1970 Lindhard dielectric function in the relaxation-time approximation *Phys. Rev.* B **1** 2362–3

[33] Stauber T, Peres N M R and Geim A K 2008 Optical conductivity of graphene in the visible region of the spectrum *Phys. Rev.* B **78** 085432
[34] Chang Y-C, Liu C-H, Liu C-H, Zhang S, Marder S R, Narimanov E E, Zhong Z and Norris T B 2016 Realization of mid-infrared graphene hyperbolic metamaterials *Nat. Commun.* **7** 10568
[35] Satou A, Vasko F T and Ryzhii V 2008 Nonequilibrium carriers in intrinsic graphene under interband photoexcitation *Phys. Rev.* B **78** 115431
[36] Peres N M R, Bludov Y V, Santos J E, Jauho A P and Vasilevskiy M I 2014 Optical bistability of graphene in the terahertz range *Phys. Rev.* B **90** 125425
[37] Yao X, Tokman M and Belyanin A 2014 Efficient nonlinear generation of thz plasmons in graphene and topological insulators *Phys. Rev. Lett.* **112** 055501
[38] Raza S, Bozhevolnyi S I, Wubs M and Mortensen N A 2015 Nonlocal optical response in metallic nanostructures *J. Phys.: Condens. Matter.* **27** 183204–20
[39] Wolff C and Mortensen N A 2018 Stimulated plasmon polariton scattering arXiv:1812.05826
[40] Raza S, Kadkhodazadeh S, Christensen T, Di Vece M, Wubs M, Mortensen N A and Stenger N 2015 Multipole plasmons and their disappearance in few-nanometer silver nanoparticles *Nat. Commun.* **6** 8788
[41] Christensen T, Wang W, Jauho A-P, Wubs M and Mortensen N A 2014 Classical and quantum plasmonics in graphene nanodisks: role of edge states *Phys. Rev.* B **90** 241414(R)
[42] Christensen T, Yan W, Jauho A-P, Soljačić M and Mortensen N A 2017 Quantum corrections in nanoplasmonics: shape, scale, and material *Phys. Rev. Lett.* **118** 157402